

## Supporting material

### **Twist angle and electric gating controllable electronic structure of two-dimensional stacked BP homo-structure**

Linwei Yao<sup>1</sup>, Jiangni Yun<sup>1\*</sup>, Peng Kang<sup>2</sup>, Hongyuan Zhao<sup>1</sup>, Siyu Zhang<sup>1</sup>, Liru Zeng<sup>1</sup>,  
Zhisong Bi<sup>1</sup>, Junfeng Yan<sup>1</sup>, Wu Zhao<sup>1</sup>, and Zhiyong Zhang<sup>1</sup>

<sup>1</sup>School of Information Science and Technology, Northwest University, Xian, 710127,  
China

<sup>2</sup>Department of Physics, McGill University, Montreal, Quebec, H3A2T8, Canada

\***E-mail address:** yjn\_calculation@163.com; niniyun@nwu.edu.cn

Table S1 Geometric parameters and structural optimization of BP monolayer. The band gap is calculated by HSE06, and the brackets represent GGA-PBE method.

	Lattice parameter (Å)			B-P bond length (Å)	Bandgap (eV)
	$a$	$b$	$\gamma$		
This work	3.213	3.213	120°	1.847	1.299(0.948)
Wang <sup>[1]</sup>	3.213	3.213	120°	1.855	1.294(0.907)

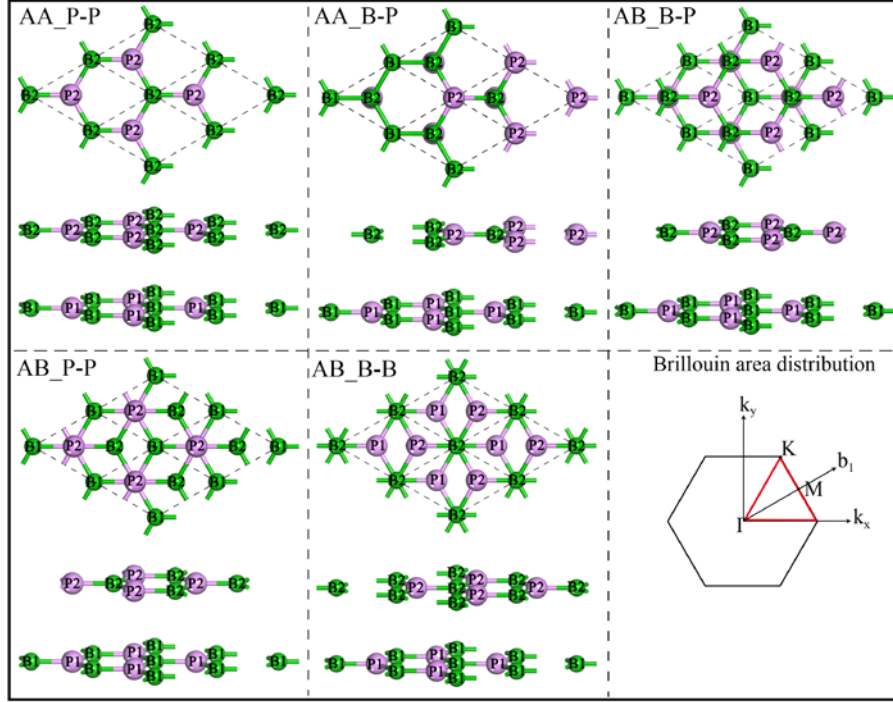


Fig. S1 Models of five stacking structures and the diagram of Brillouin area distribution.

AA\_P-P (bottom B atoms and P atoms are located directly above B atoms and P atoms, respectively), AA\_B-P (bottom B atoms and P atoms are located directly above P atoms and B atoms, respectively), AB\_B-P (bottom B atoms and B atoms are located directly above atom and P atom are located directly above the six-membered ring and B atom, respectively), AB\_P-P (the underlying B atom and P atom are located directly above the six-membered ring and P atom, respectively), AB\_B-B (bottom B and P atoms are located directly above the center of the six membered ring, respectively).

Table S2 Calculated interlayer distance ( $d$ ), the energy difference relative to formation energy ( $E_f$ ), binding energy ( $E_b$ ), and band-gap ( $E_g$ ) of BP bilayer with different stacking structures. The band gap is calculated by HSE06, and the brackets represent the GGA-PBE method.

Structure	$d$ (Å)	$E_f$ (meV/atom)	$E_b$ (meV/Å <sup>2</sup> )	$E_g$ (eV)
AA_P-P	3.997	-31.93	-12.67	0.230(0.184)
AA_B-P	3.879	-38.97	-15.81	0.841(0.793)
AB_B-P	3.605	-47.12	-19.42	1.036(0.579)
AB_P-P	3.779	-37.66	-15.22	0.378(0.330)
AB_B-B	3.627	-45.36	-18.62	0.408(0.361)

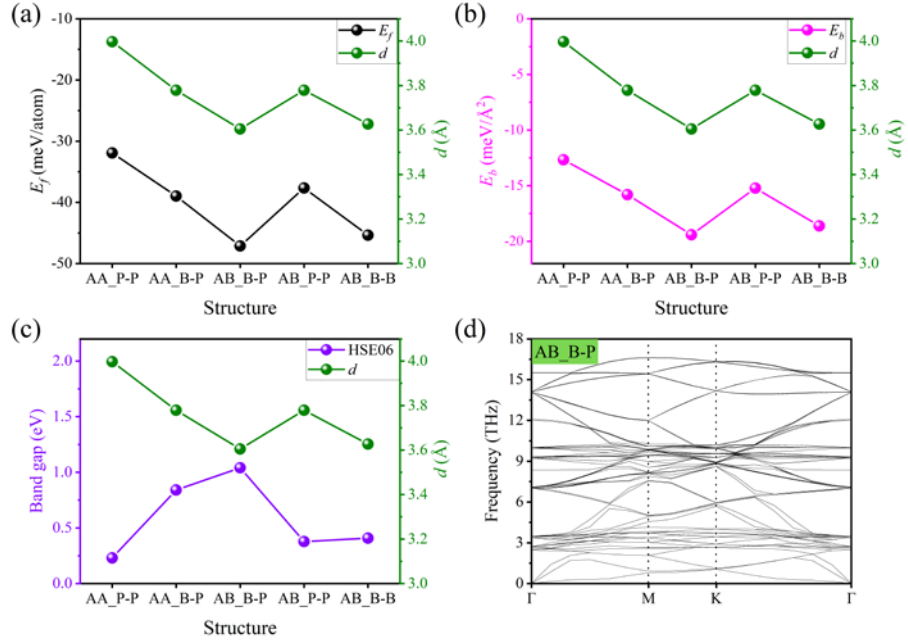


Fig. S2 (a)-(c) show the relationship between layer spacing and formation energy, binding energy, bandgap, and (d) the phonon dispersion curve of AB\_B-P, respectively.

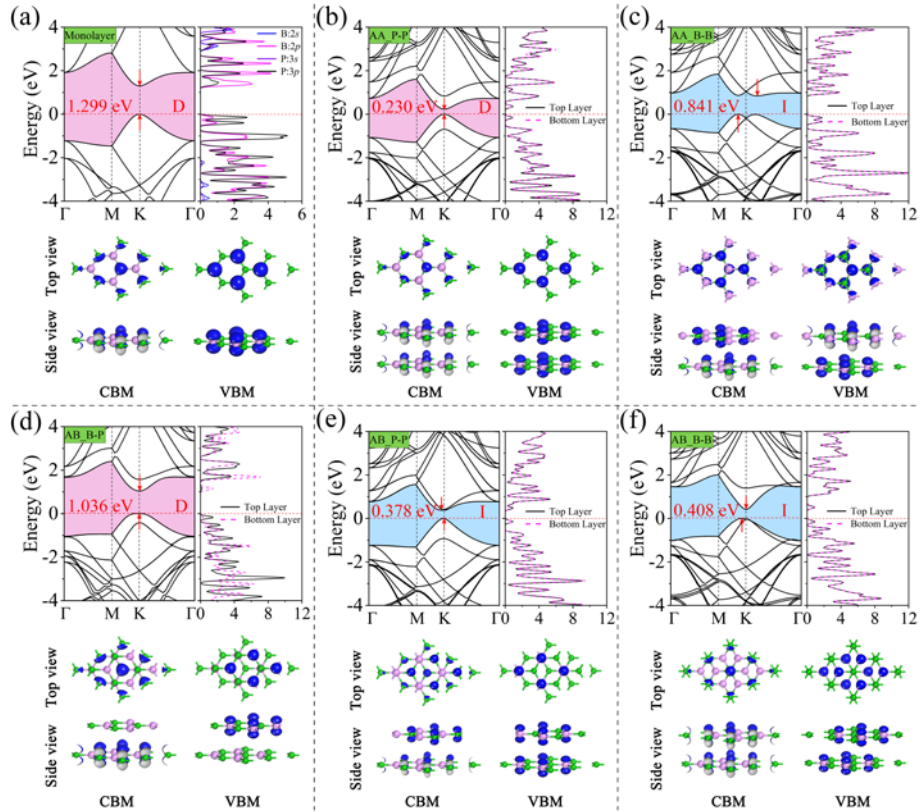


Fig. S3 (a)-(f) show band structure and charge distribution of CBM and VBM of monolayer BP and five kinds of stacks.

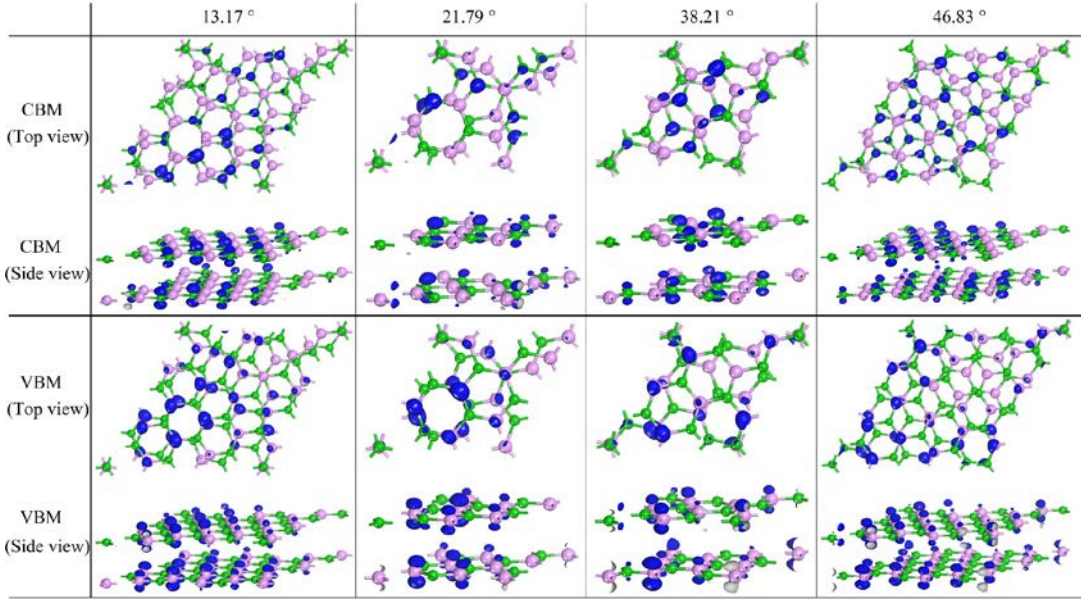


Fig. S4 Wave function distributions of bottom conduction band and top valence band for four kinds of torsional structures.

Twist angle models were created using the builder interface in Virtual Nanolab (VNL). [2]

The measured data of  $E_I$  are shown in Tables S3-S6, where  $E_{CB}$  and  $E_{VB}$  are the energy values of the bottom of the conduction band and the top of the valence band in the energy band diagram, both of which can be read directly in the energy band diagram. Since the software sets  $E_{VB}$  at 0 eV by default during calculation,  $E_{VB}=0$  eV. Where  $E_I=\partial E_d/\partial \delta$ ,  $E_{d(CB)}=E_{CB}-E_V$ ,  $E_{d(VB)}=E_{VB}-E_V$ ,  $E_V$  is the vacuum energy level,  $\delta=\Delta l/l_0$ ,  $\Delta l$  is the amount of lattice change,  $l_0$  is the crystal lattice parameter.

Table S3 Determination of the relevant data of the deformation potential constant ( $E_I$ ) of the monolayer BP along the zigzag direction.

$\delta$	$E_{CB}$ (eV)	$E_{VB}$ (eV)	$E_V$ (eV)	$E_{d(CB)}$ (eV)	$E_{d(VB)}$ (eV)
0.020	0.883	0.000	5.045	-4.162	-5.045
0.015	0.864	0.000	5.010	-4.146	-5.010
0.010	0.851	0.000	4.996	-4.145	-4.996
0.005	0.871	0.000	5.000	-4.129	-5.000
0.000	0.851	0.000	4.961	-4.110	-4.961
-0.005	0.833	0.000	4.943	-4.110	-4.943
-0.010	0.834	0.000	4.949	-4.115	-4.949
-0.015	0.821	0.000	4.914	-4.093	-4.914
-0.020	0.810	0.000	4.899	-4.089	-4.899

Table S4 Determination of the relevant data of the deformation potential constant ( $E_I$ ) of the monolayer BP along the armchair direction.

$\delta$	$E_{CB} (eV)$	$E_{VB} (eV)$	$E_V (eV)$	$E_{d(CB)} (eV)$	$E_{d(VB)} (eV)$
0.020	0.849	0.000	5.018	-4.169	-5.018
0.015	0.846	0.000	5.001	-4.155	-5.001
0.010	0.846	0.000	4.975	-4.129	-4.975
0.005	0.859	0.000	4.989	-4.130	-4.989
0.000	0.851	0.000	4.961	-4.110	-4.961
-0.005	0.856	0.000	4.975	-4.119	-4.975
-0.010	0.844	0.000	4.940	-4.096	-4.940
-0.015	0.825	0.000	4.921	-4.096	-4.921
-0.020	0.809	0.000	4.920	-4.089	-4.920

Table S5 Determination of the relevant data of the deformation potential constant ( $E_I$ ) of the AB\_B-P ( $0^\circ$ ) structure along the zigzag direction.

$\delta$	$E_{CB} (eV)$	$E_{VB} (eV)$	$E_V (eV)$	$E_{d(CB)} (eV)$	$E_{d(VB)} (eV)$
0.020	0.611	0.000	4.933	-4.322	-4.933
0.015	0.598	0.000	4.920	-4.322	-4.920
0.010	0.584	0.000	4.904	-4.320	-4.904
0.005	0.580	0.000	4.880	-4.300	-4.880
0.000	0.564	0.000	4.879	-4.315	-4.879
-0.005	0.574	0.000	4.877	-4.303	-4.877
-0.010	0.592	0.000	4.882	-4.290	-4.882
-0.015	0.590	0.000	4.864	-4.274	-4.864
-0.020	0.590	0.000	4.860	-4.270	-4.860

Table S6 The relevant data of the determination of the deformation potential constant ( $E_I$ ) of the AB\_B-P ( $0^\circ$ ) structure along the armchair direction.

$\delta$	$E_{CB} (eV)$	$E_{VB} (eV)$	$E_V (eV)$	$E_{d(CB)} (eV)$	$E_{d(VB)} (eV)$
0.020	0.566	0.000	4.911	-4.3454	-4.911
0.015	0.565	0.000	4.907	-4.342	-4.907
0.010	0.564	0.000	4.892	-4.328	-4.892
0.005	0.564	0.000	4.886	-4.322	-4.886
0.000	0.564	0.000	4.879	-4.315	-4.879
-0.005	0.565	0.000	4.876	-4.311	-4.876
-0.010	0.566	0.000	4.866	-4.300	-4.866
-0.015	0.567	0.000	4.860	-4.293	-4.860
-0.020	0.568	0.000	4.855	-4.287	-4.855

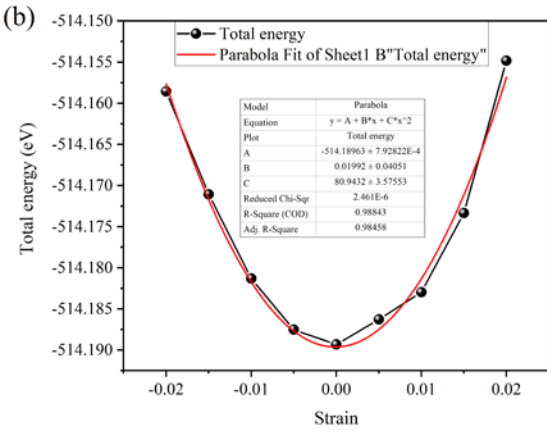
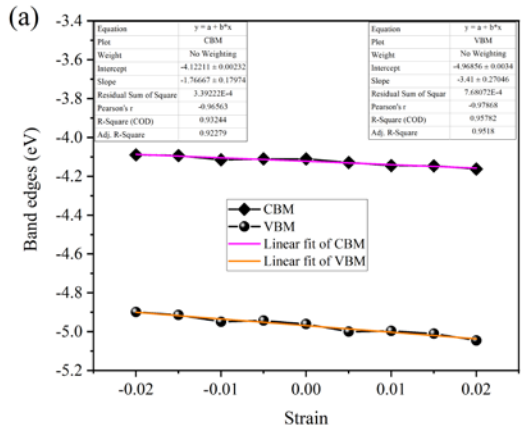
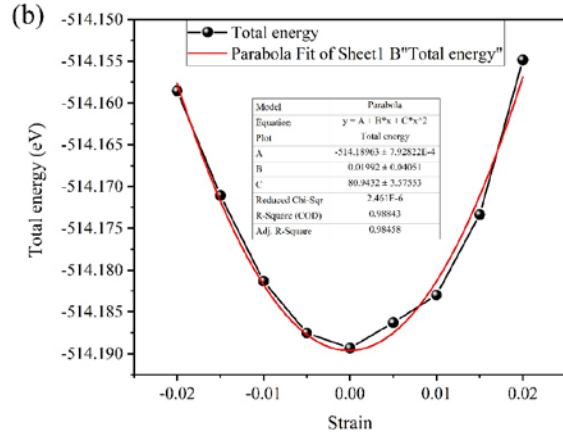
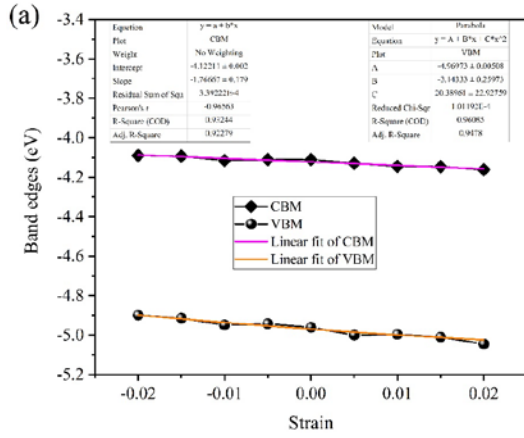
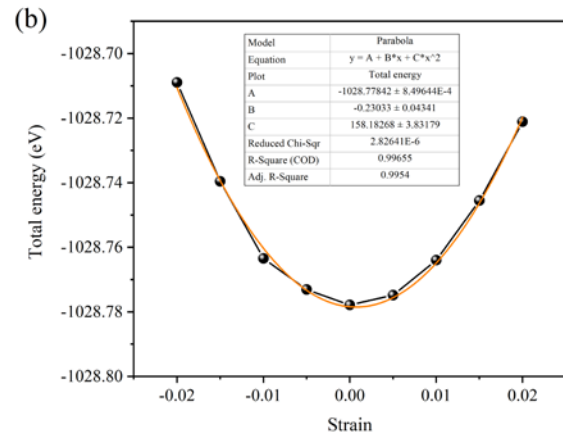
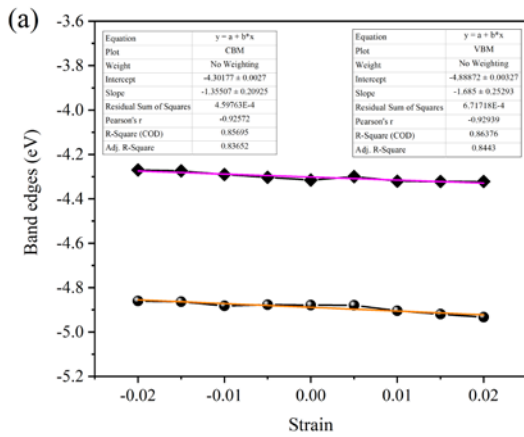


Fig. S5 Monolayer BP as a function of applying uniaxial compression or tension along the zigzag direction, (a) deformation potential constant  $E_I$  of CBM and VBM, (b), and elasticity modulus along the armchair direction, (c) deformation potential constant  $E_I$  of CBM and VBM, (d) elasticity modulus along the armchair direction.



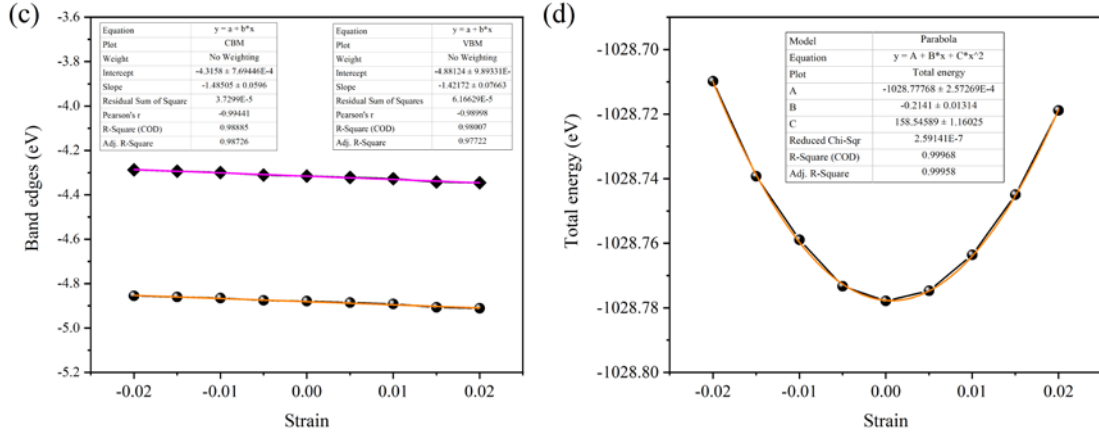


Fig. S6 AB<sub>B</sub>-P (0°) as a function of applying uniaxial compression or tension along the zigzag direction, (a) deformation potential constant  $E_I$  of CBM and VBM, (b), and elasticity modulus along the armchair direction, (c) deformation potential constant  $E_I$  of CBM and VBM, (d) elasticity modulus along the armchair direction.

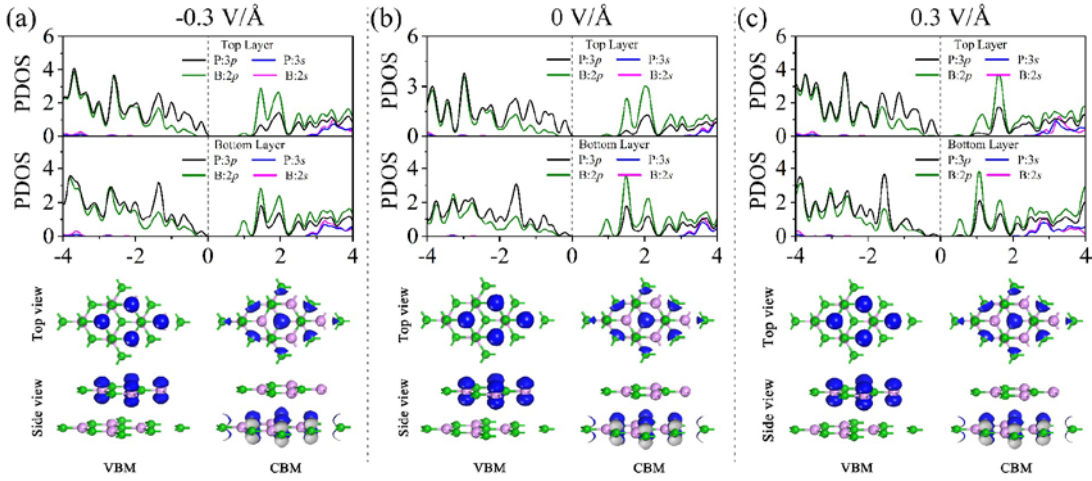


Fig. S7 PDOS, CBM and VBM of 0° structure under (a) -0.3 V/Å, (b) 0.0 V/Å and (c) 0.3 V/Å electric fields, respectively.

As we known, in first-principles calculation, when an external electricity field is applied to the surface of the two-dimensional material, the vacuum layer is used as the dielectric layer. Therefore, at the vacuum layer, the gradient of electrostatic potential under an external electric field indicates the strength of the external electric field.

To demonstrate this viewpoint, as presented in Fig. S8, we use the convergence position at 0 V/Å as the O (L) point, and pass the O (L) point to make a horizontal black dotted line, and then intersect with the electrostatic curve under other electric fields to O1 (P1), O2 (P2), and O3 (P3), O4 (P4), O5 (P5), O6 (P6), and then make vertical black dotted lines for each Ox point, hand in L1, L2, L3, L4, L5, L6. Then we calculate the slope of OxPx, and the results are shown in Table S7. The results show that the slope of the tilted straight line at both ends of the electrostatic potential indicates the strength of the electric field.

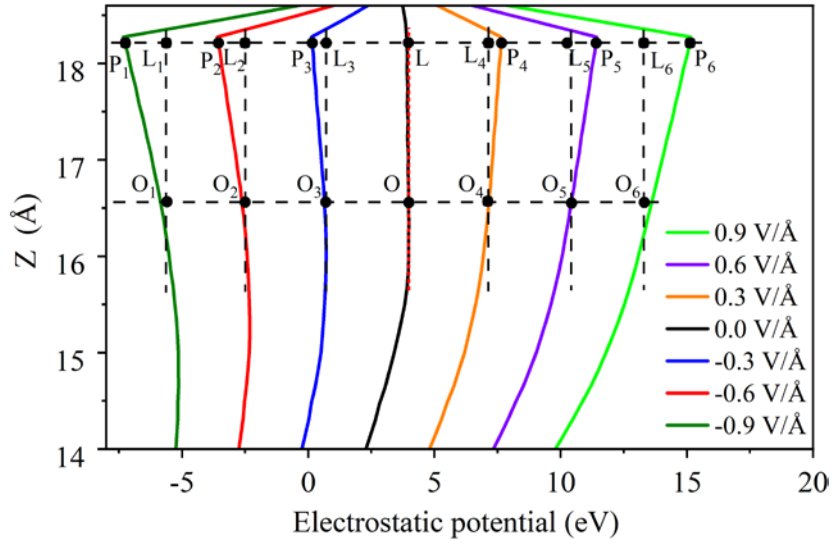


Fig. S8 Electrostatic potential distribution of the  $0^\circ$  structure under  $18.5 \text{ \AA}$  vacuum layer.

Table S7 The coordinates and slope of the  $P_x$  ( $O_x$ ) ( $x = 1, 2, 3, 4, 5, 6$ ) under different electric fields.

	-0.9 V/Å	-0.6 V/Å	-0.3 V/Å	0.0 V/Å	0.3 V/Å	0.6 V/Å	0.9 V/Å
<b>P<sub>x</sub></b>	(18.103, -7.232)	(18.103, -3.552)	(18.103, 0.172)	(18.103, 3.897)	(18.103, 7.615)	(18.103, 11.345)	(18.103, 15.000)
<b>O<sub>x</sub></b>	(16.551, -5.850)	(16.551, -2.627)	(16.551, 0.635)	(16.551, 3.894)	(16.551, 7.145)	(16.551, 10.408)	(16.551, 13.600)
<b>Slope</b>	-0.892	-0.596	-0.298	0.001	0.302	0.603	0.904

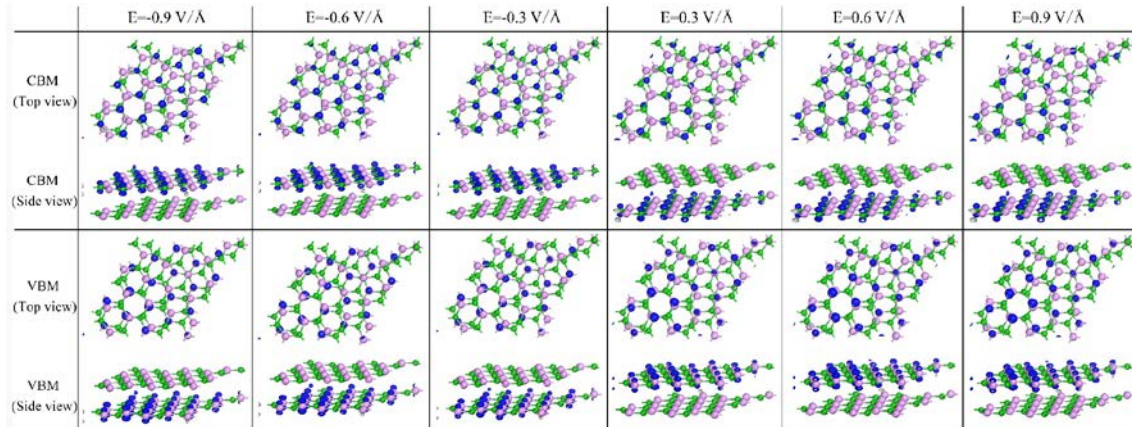


Fig. S9 Wave function distribution of CBM and VBM with  $13.17^\circ$  structure under different positive and negative electric fields.

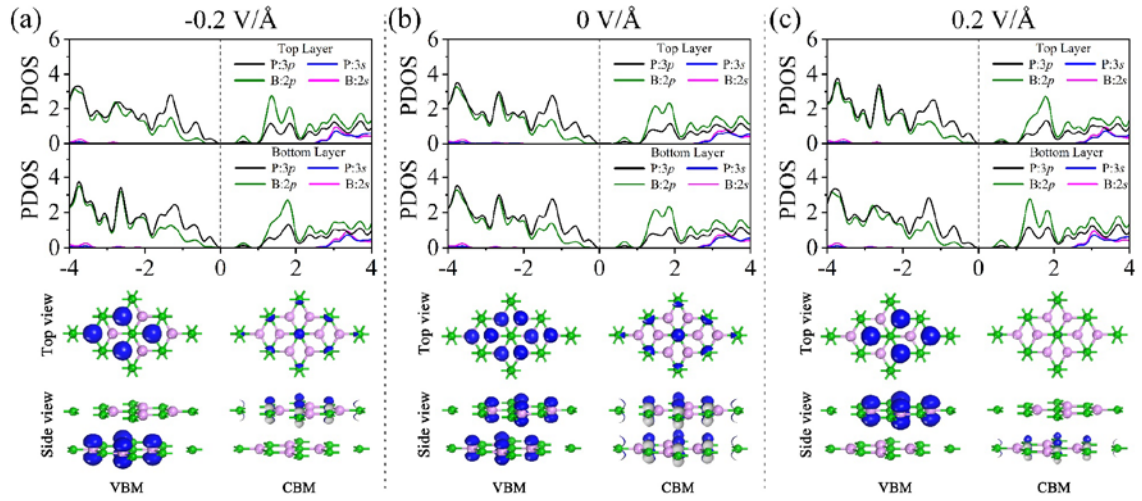


Fig. S10 PDOS, CBM and VBM of  $60^\circ$  structure under electric fields (a)  $-0.2 \text{ V/\AA}$ , (b)  $0 \text{ V/\AA}$  and (c)  $0.2 \text{ V/\AA}$ , respectively.

## Reference

- [1] Wang Y, Huang C, Li D, et al. *Journal of Physics: Condensed Matter*, 2019, 31(46): 465502.
- [2] Virtual NanoLab version 2015.1, QuantumWise A/S ([www.quantumwise.com](http://www.quantumwise.com)).